THE JOURNAL OF PHYSICAL CHEMISTRY A

Article

pubs.acs.org/JPCA

Isoprene NO_3 Oxidation Products from the RO_2 + HO_2 Pathway

Rebecca H. Schwantes,[*,†] Alexander P. Teng,[†] Tran B. Nguyen,[†] Matthew M. Coggon,[‡] John D. Crounse,[†] Jason M. St. Clair,[∥,⊥] Xuan Zhang,[†] Katherine A. Schilling,[‡] John H. Seinfeld,[‡,§] and Paul O. Wennberg[*,†,§]

[†]Division of Geological and Planetary Sciences, California Institute of Technology, 1200 East California Boulevard, Pasadena, California 91125, United States

[‡]Division of Chemistry and Chemical Engineering, California Institute of Technology, 1200 East California Boulevard, Pasadena, California 91125, United States

[§]Division of Engineering and Applied Science, California Institute of Technology, 1200 East California Boulevard, Pasadena, California 91125, United States

[∥]Atmospheric Chemistry and Dynamics Laboratory, NASA Goddard Space Flight Center, Greenbelt, Maryland 20771, United States

[⊥]Joint Center for Earth Systems Technology, University of Maryland Baltimore County, Baltimore, Maryland 21250, United States

Supporting Information

ABSTRACT: We describe the products of the reaction of the hydroperoxy radical (HO_2) with the alkylperoxy radical formed following addition of the nitrate radical (NO_3) and O_2 to isoprene. NO_3 adds preferentially to the C_1 position of isoprene (>6 times more favorably than addition to C_4), followed by the addition of O_2 to produce a suite of nitrooxy alkylperoxy radicals (RO_2). At an RO_2 lifetime of ∼30 s, δ-nitrooxy and β-nitrooxy alkylperoxy radicals are present in similar amounts. Gas-phase product yields from the RO_2 + HO_2 pathway are identified as 0.75−0.78 isoprene nitrooxy hydroperoxide (INP), 0.22 methyl vinyl ketone (MVK) + formaldehyde (CH_2O) + hydroxyl radical (OH) + nitrogen dioxide (NO_2), and 0−0.03 methacrolein (MACR) + CH_2O + OH + NO_2. We further examined the photochemistry of INP and identified propanone nitrate (PROPNN) and isoprene nitrooxy hydroxyepoxide (INHE) as the main products. INHE undergoes similar heterogeneous chemistry as isoprene dihydroxy epoxide (IEPOX), likely contributing to atmospheric secondary organic aerosol formation.

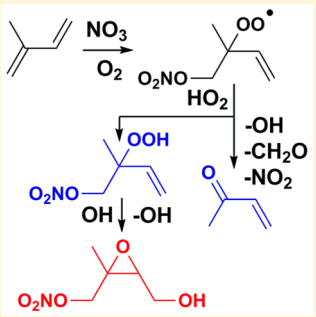

1.0. INTRODUCTION

NO_3 oxidation of alkenes typically occurs during the night because NO_3 readily photolyzes under solar radiation. Daytime NO_3 chemistry can, however, be important under conditions in which NO_3 photolysis is suppressed (e.g., below dense clouds or in thick forest canopies). The oxidation of isoprene, the most abundantly emitted alkene in the atmosphere, is of particular interest to global climate and tropospheric chemistry. While the rate of isoprene emission is low at night,[1,2] isoprene can accumulate in the boundary layer in the late afternoon when OH concentrations have diminished.[3−8] Although nighttime isoprene concentrations are highly variable, its mixing ratio has been measured to be as high as several ppb just before sunset, and upon nightfall, typically declines, widely attributed to reaction with NO_3.[3,4]

The rate of NO_3 formation is controlled by the concentrations of nitrogen dioxide (NO_2), O_3, and temperature. In heavily populated urban areas, e.g., the Northeast United States, the NO_3 mixing ratio can approach 300 ppt during the night in the summer.[9] At night, OH concentrations approach zero, so isoprene will react either with NO_3 or O_3. Even when NO_3 mixing ratios are 10^4 times lower than those of O_3, reaction of isoprene with NO_3 is still competitive due to the large disparity in the reaction rate constants of isoprene with O_3 (1.3×10^{-17} cm^3 $molecule^{-1}$ s^{-1})[10] and NO_3 (7.0×10^{-13} cm^3 $molecule^{-1}$ s^{-1})[11] at 298 K.

Organic nitrates are the major product of the reaction of isoprene with NO_3 (65−80%).[12−18] On the basis of this high nitrate yield, Horowitz et al.[19] predicted that, in the Southeast United States, 50% of the isoprene nitrates are derived from NO_3 chemistry, even though this process represents only 6% of isoprene loss. Using an updated mechanism of the community multiscale air quality (CMAQ) model, Xie et al.[20] also predicted that a large portion of isoprene nitrates are attributable to NO_3 oxidation (∼40%). Thus, isoprene NO_3 chemistry is important for understanding how formation of organic nitrogen impacts regional NO_x and O_3 concentrations. Indeed in forested regions that are influenced by urban emissions, the formation of these nitrates in the oxidation of isoprene by NO_3 can be a significant sink for NO_x.

Organic nitrates are likely involved in secondary organic aerosol (SOA) formation. Using SOA yield measurements from

Received: July 2, 2015
Revised: August 27, 2015
Published: September 3, 2015

DOI: 10.1021/acs.jpca.5b06355
J. Phys. Chem. A 2015, 119, 10158−10171

Table 1. List of Isoprene NO_3 Oxidation Chamber Experiments

expt no.	chamber size (m^3)	CH_2O (ppm)	NO_2 (ppb)	O_3 (ppb)[a]	isoprene (ppb)	seed type[b]	RH (%)
1	24	2.1	300	152, ~50	80	none	31−41
2	24	2.2	300	155, ~50	80	$(NH_4)_2SO_4$	34−42
3	24	2.2	300	157, ~50	80	$MgSO_4$, H_2SO_4	<3−6
4	24	2.2	300	160, ~50	80	$(NH_4)_2SO_4$	<3−7
5	24	2.2	300	152, ~50	80	none	<3−3
6	24	4.7	300	153, ~50, ~50	60	$MgSO_4$, H_2SO_4	<3−5
7	1	2.0	330	~150, ~50	85	none	−
8	1	4.0	100	49	24	none	−
9	24	4.1	100	49	18	none	<3−9
10	1	0	100	0	97	none	−

[a]Multiple injections of O_3 occurred in some experiments. O_3 mixing ratios are listed according to injection order. [b]The atomizing solutions for the seed types used in this experiment were: 0.06 M $(NH_4)_2SO_4$ and 0.03 M $MgSO_4$ + 0.03 M H_2SO_4.

chamber studies, Brown et al.[7] estimate that isoprene NO_3 chemistry contributes more to SOA formation than isoprene OH chemistry in urban areas of the Northeast United States. Rollins et al.[21] observed that the particulate nitrate fraction and total organic aerosol mass concentration are enhanced at night, implicating nitrates from NO_3 oxidation as the cause.

Isoprene oxidation by NO_3 leads to the formation of peroxy radicals (RO_2), and the subsequent chemistry will depend on which radical these RO_2 react with (e.g., RO_2, HO_2, NO_3). Atmospherically relevant studies of NO_3 oxidation of biogenic compounds require radical conditions similar to those encountered in forested environments. Measured HO_2 concentrations at night are often several ppt.[22] For example, during the BEARPEX 2009 field campaign (located 75 km northeast of Sacramento, CA), the HO_2 mixing ratio at night was ~4 ppt,[23] while NO_3 was only ~1 ppt.[24] Model calculations conducted by Xie et al.[20] using CMAQ suggest that nearly half of the RO_2 reacts with HO_2 in the nighttime boundary layer. Consistent with these simulations, isoprene nitrooxy hydroperoxide (INP), a product from the RO_2 + HO_2 pathway, was detected during the BEARPEX 2009[8] and the Southern Oxidant and Aerosol Study (SOAS) 2013 field campaigns with a diurnal pattern consistent with a nighttime source (see section 5.0). These findings support the importance of the RO_2 + HO_2 pathway in the atmospheric oxidation of isoprene by NO_3.

To date, NO_3 radicals in laboratory chamber studies have been produced either via decomposition of N_2O_5 or via reaction of O_3 and NO_2. In these studies, a significant fraction of the isoprene derived alkylperoxy radicals (RO_2) react with either NO_3 or with other RO_2, which is dissimilar to the chemistry in most forested environments. In this study, we investigate the oxidation of isoprene by NO_3 in the presence of considerably higher concentrations of HO_2 radicals. We further investigate the photooxidation of the nitrates produced in this chemistry to understand the potential reactive uptake of these compounds to the particle phase.

2.0. EXPERIMENTAL METHODS

We examined the products formed from NO_3 oxidation of isoprene in an environmental chamber. To study the RO_2 + HO_2 pathway, formaldehyde (CH_2O) was injected into the chamber along with NO_2 and O_3 to enhance HO_2 production. The basic reactions summarizing the chemistry for this approach are shown below R1−R6. Table SA2 includes a more comprehensive list of general reactions.

$$O_3 + NO_2 \rightarrow NO_3 + O_2 \quad \text{(R1)}$$

$$NO_3 + CH_2O \rightarrow HNO_3 + CHO \quad \text{(R2)}$$

$$CHO + O_2 \rightarrow HO_2 + CO \quad \text{(R3)}$$

$$HO_2 + NO_2 + M \rightleftharpoons HO_2NO_2 + M \quad \text{(R4)}$$

$$NO_2 + NO_3 + M \rightleftharpoons N_2O_5 + M \quad \text{(R5)}$$

$$HO_2 + HO_2 \rightarrow H_2O_2 + O_2 \quad \text{(R6)}$$

This chemistry represents a new approach for studying NO_3 oxidation with an independent HO_2 source. It mimics atmospheric conditions in forested environments more closely than previous studies. With this approach, formation of NO_3 and HO_2 are coupled such that a nearly constant ratio of NO_3 to HO_2 is maintained throughout the experiment.

2.1. Experimental Procedures. All experiments were carried out in either a 24 m^3 or a 1 m^3 Teflon chamber (see Table 1 for a list of experiments). Prior to each experiment, the 24 m^3 chamber was flushed with purified, dry air for 24 h such that all volatile organic compounds were below the detection limit, particle number concentration was <10 cm^{-3}, and particle volume concentration was <0.01 μm^3 cm^{-3}. Prior to each of the 1 m^3 experiments, the chamber was filled and flushed repetitively until all gas-phase products were below the detection limit.

For experiments 1 and 2, the chamber was humidified prior to all injections. Dry, purified air was passed through a Nafion membrane humidifier (FC200, Permapure LLC) that is kept wet by recirculation of 27 °C ultrapure water (18MΩ, Millipore Milli-Q). O_3 was introduced by flowing dry, purified air through an ozone generator (EMMET).

Gas phase CH_2O was produced by flowing N_2 over paraformaldehyde solid (97% purity) in a heated glass bulb and subsequently through a 0 °C trap to remove impurities. The CH_2O was finally condensed and stored in a trap submerged in liquid nitrogen. CH_2O was injected into the chamber after introduction of O_3 by filling a glass bulb with several Torr of pure CH_2O and backfilling with dry N_2 gas. The final concentration in the glass bulb was ~1−2% CH_2O. The CH_2O mixing ratio in the bulb was measured using Fourier transform infrared spectroscopy (calculated from the HITRAN line list) and found to agree within ~14% of the concentration calculated from manometry. The mixing ratio in the bulb, however, decreased slowly over time indicating that some loss due to CH_2O polymerization or deposition to the walls of the bulb occurs at these concentrations. Thus, CH_2O was injected

DOI: 10.1021/acs.jpca.5b06355
J. Phys. Chem. A 2015, 119, 10158−10171

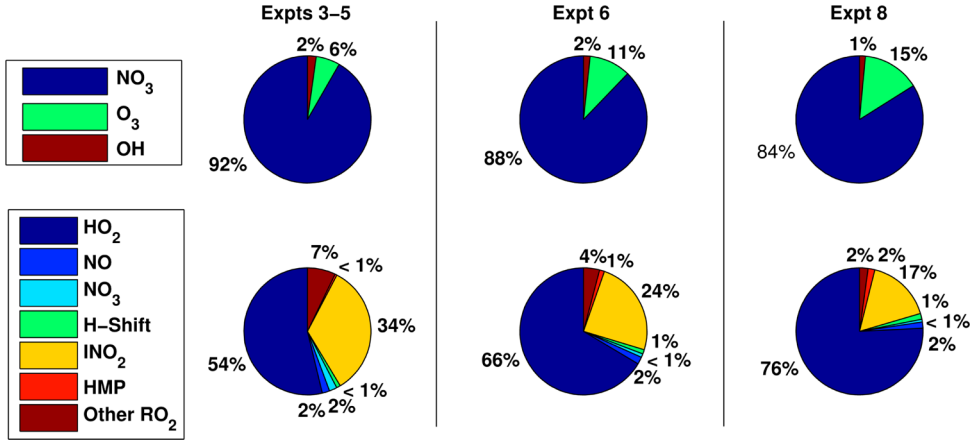

Figure 1. Isoprene reactant partner distribution (top graphs), and the nitrooxy alkylperoxy (INO_2) radical reactant partner distribution (bottom graphs) predicted by the kinetic mechanism (section S1). Abbreviations not yet defined are hydroxy methyl peroxy radical (HMP).

immediately into the chamber after the bulb was prepared to prevent further loss. For the ∼24 m^3 chamber, the CH_2O values reported in Table 1 were calculated assuming that the chamber volume was consistent for each experiment. With the exception of experiment 9, CH_2O was not measured in the chamber.

NO_2 (488 ppm in N_2, Scott Specialty Gases) was directly injected into the chamber through a mass flow controller. After 1 h, sufficient amounts of NO_3 and HO_2 were generated, and isoprene (99% purity) was introduced by injecting a known volume into a glass bulb fitted with a septum and flowing purified, clean air through the bulb into the chamber. The mixing ratios of NO_3 and HO_2 prior to isoprene injection varied by experiment, but as an example, the kinetic mechanism for experiment 8 predicts ∼10 ppt NO_3 and ∼70 ppt HO_2.

For standard NO_3 oxidation experiments (1−5), additional O_3 was injected in the dark after 2.5−3 h of reaction to oxidize the remaining isoprene. After an additional 2.5−3 h, the UV lights were turned on ($j_{NO_2} = 5 \times 10^{-3}$ s^{-1}) for 3 h to generate OH and photochemically oxidize the first-generation nitrates. Seed aerosols were subsequently introduced into the chamber (after 1 h dark equilibrium) to test SOA formation. To inject seed particles, dilute (0.03−0.06 M) aqueous solutions of various salts (Table 1) were atomized through a ^{210}Po neutralizer into the chamber. For humid experiments, the seeds were hydrated prior to injection into the chamber with a wet-wall denuder heated to ∼90 °C.

For experiment 6, O_3 was added 6.5 h after isoprene injection and then again 3 h later, in order to monitor second-generation products from NO_3 oxidation. At the end of experiment 6, highly acidic seed was injected to investigate those products formed prior to photooxidation that undergo reactive uptake to seed aerosol. Experiments 7 and 8 were run in a 1-m^3 Teflon chamber ($j_{NO_2} = 2.5 \times 10^{-3}$ s^{-1}). For experiment 7, all procedures were the same as the standard NO_3 experiments (1−5) described above. In experiment 8, more CH_2O, and less isoprene, O_3, and NO_2 were added to the chamber in order to slow down the chemistry and increase the fraction of isoprene reacting via the $RO_2 + HO_2$ pathway. Experiment 9 was run in the same way as experiment 8, but carried out during the Focused Isoprene eXperiment at the California Institute of Technology (FIXCIT) campaign.[25] For experiment 10, second-generation chemistry was further minimized by injecting isoprene along with methyl nitrite (160 ppb), NO_2, and H_2O_2 (3.2 ppm) to create conditions in the chamber containing several oxidants (NO_3, HO_2, OH, and NO). After an initial photooxidation period (52 min, $j_{NO_2} = 9.4 \times 10^{-5}$ s^{-1}) to generate HO_2, lights were turned off and isoprene NO_3 oxidation began.

Figure 1 details the predicted isoprene oxidation fate and the nitrooxy alkylperoxy radical fate for a subset of the experiments (Table 1). To minimize the $RO_2 + RO_2$ chemistry, we find that the CH_2O/isoprene ratio should be high (>70 in experiments 6 and 8). Experiment 8 had the most optimal conditions because the $RO_2 + HO_2$ pathway was clearly favored over the $RO_2 + RO_2$ pathway, and background OH was sufficiently small to limit second-generation chemistry that would not typically occur at night in the ambient atmosphere. This study focuses mainly on results from experiment 8. See the Supporting Information for analysis of the other experiments.

2.2. Instrumentation. A gas chromatograph with a flame ionization detector (GC-FID, HP 6890N) using a HP-Plot-Q column was used to monitor isoprene, methyl vinyl ketone (MVK) and methacrolein (MACR). A −40 °C cold trap upstream of the GC-FID was used to discriminate between authentic carbonyls and interfering hydroperoxides/epoxides.[26,27] The cold trap was warmed, cleaned, and dried every 2−3 h to avoid occluding sample flow with ice build-up. The cold trap was not used for experiments with high RH. Without the cold-trap, interferences increased MVK and MACR signals by ∼10 and ∼2 fold, respectively, suggesting that other hydroperoxides, such as INP, also interfere with the GC-FID detection of MVK and MACR in a manner similar to that observed for the first generation hydroxy hydroperoxides formed via oxidation of isoprene by OH (ISOPOOH).[26,27]

Relative humidity (RH) and temperature were monitored via a Vaisala HMM211 probe. O_3 was monitored using a Horiba O_3 analyzer (APOA-360). NO_2 and NO were monitored using a Teledyne NO_x analyzer (Teledyne T200). Particle volume was monitored via a differential mobility analyzer (TSI, 3081) coupled with a condensation particle counter (TSI, 3010), and particle composition was monitored by a time-of-flight aerosol mass spectrometer (AMS) (Aerodyne Research, Inc.).[28] AMS data were processed using software (Squirrel 1.51H)[29] with updated O:C ratios recommended by Canagaratna et al.[30] The collection efficiency (0.75) in this work was assumed to be the same as that calculated for IEPOX derived organic aerosol.[31]

A chemical ionization mass spectrometer (CIMS) using a custom−modified triple quadrupole mass analyzer (Varian,

DOI: 10.1021/acs.jpca.5b06355
J. Phys. Chem. A 2015, 119, 10158−10171

1200)[32] was used to monitor gaseous oxidized organic species. The CIMS uses CF_3O^- as the reagent ion. CF_3O^- interacts with an analyte (A) in either a transfer reaction (generally acidic species, R7) or a cluster complex (R8):[32−34]

$$CF_3O^- + A \rightarrow CF_2O + A^-_{(-H)}\cdot HF \quad (R7)$$

$$CF_3O^- + A \rightarrow CF_3O^-\cdot A \quad (R8)$$

MS/MS mode was used on the triple quadruple CIMS to separate isobaric compounds such as ISOPOOH and dihydroxy epoxide (IEPOX).[33] In addition to a triple quadruple CIMS (triple-CIMS), a time-of-flight CIMS (ToF-CIMS) coupled to a GC[35−37] was used during experiments 7−10. GC separation was achieved by cryofocusing products at the head of a 1m or 4 m GC column (RTX-1701 megabore) with a ∼−25 °C 2-propanol cold bath. The oven temperature was set to ramp from 30 to 60 °C at 3 °C/min and 60−120 °C at 10 °C/min. Elution of products from the GC was monitored with the ToF- or triple-CIMS.

As synthetic standards are not available, the CIMS sensitivities for most of the isoprene nitrates formed in this work are not known. The large isoprene nitrates (CF_3O^- cluster ions with $m/z \geq (-)$ 230 except (−) 234, for which the sensitivity has been measured) were assumed to have the same sensitivity as IHN that was previously quantified using synthetic standards.[25,38] The uncertainty in the ToF-CIMS sensitivities is ±20% for IHN. On the basis of theoretical calculations of the dipole moment and polarizability of the main nitrates (Kwan et al.[15] (INP and ICN) and Paulot et al.[18] (IHN)), the sensitivities are expected to be similar, so we do not expect the uncertainty for the large nitrates formed in this work to exceed ±20%. For non-nitrate species and the smaller nitrate species, synthesized standards or those of structurally similar compounds were used to calibrate the ToF-CIMS (measurement uncertainties ±20%).

3.0. RESULTS

The general isoprene−NO_3 reaction mechanism is shown in Scheme 1. Four of the six nitrooxy alkylperoxy radical isomers are shown. The two *cis*-δ products also form, but for brevity are not shown. Structural isomers are named according to the oxidant addition site (first number) and O_2 addition site (second number) on the isoprene skeleton (see Scheme 1 for examples). For clarity, isoprene hydroxy nitrates (IHN) are labeled with an N next to the carbon number at which the nitrate group is attached since they arise from both OH and NO_3 oxidation. Photooxidation products of the dominant β- and δ-INP are shown in Scheme 2.

The main first-generation products formed from NO_3 oxidation of isoprene are C_5 nitrooxy hydroperoxide (INP), C_5 carbonyl nitrate (ICN), and C_5 hydroxy nitrate (IHN) (Figure 2 and Table 2). The molar yield of INP is higher than found in previous studies (Table 2), likely due to the significantly higher ratio of HO_2 to NO_3 in these experiments. The total molar yield of organic nitrates is estimated to be 76 ± 15% (Table 2) of isoprene reacted; this includes isoprene loss due to O_3 (∼15%, see Figure 1), which presumably does not form nitrates. The nitrate yield determined in this study is similar to previous studies, which reported organic nitrate yields ranging from 65−80%.[12−15] The product yields from other studies are also included as reference in Table 2, but comparing these yields directly is not possible because the contributions of $RO_2 + HO_2$, $RO_2 + RO_2$, and $RO_2 + NO_3$ are not equal between the studies. Refer to Figure 1 for the contribution of each pathway predicted by the kinetic mechanism for a subset of experiments in this study.

We quantify isomer specific yields of the main nitrates formed using the GC-ToF-CIMS (Table 3). INP fragments during ionization (∼12%) in the CF_3O^- CIMS. Data in Table 2 and Table 3 are corrected for this fragmentation (see S3.0 for more details). We use experiment 8 to determine the isomer-dependent yields for ICN and IHN because this experiment

Scheme 1. Diagram of the Main Products Formed from NO_3 Oxidation of Isoprene

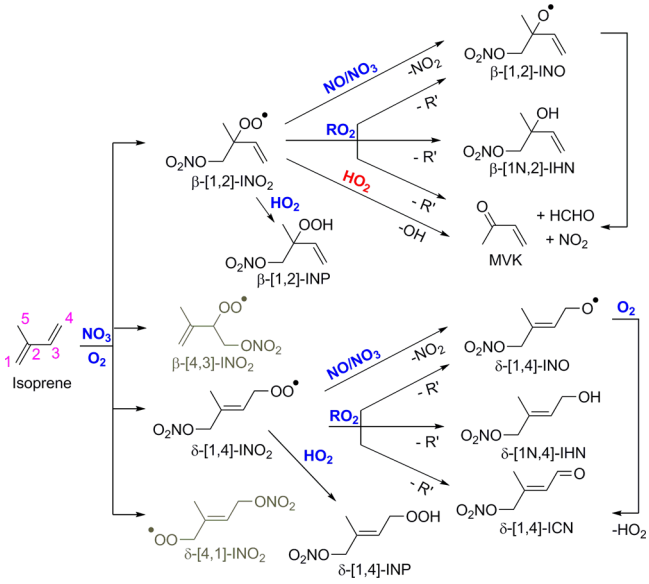

For simplicity, products from only the dominant β and δ isomer are presented. Well-established reactions are in blue. New or previously proposed reactions are in red.[13,15] Carbon atom numbers for isoprene are shown in magenta. Acronyms used are nitrooxy alkylperoxy radical (INO_2), nitrooxy alkoxy radical (INO), C_5 nitrooxy hydroperoxide (INP), C_5 hydroxy nitrate (IHN), methyl vinyl ketone (MVK), and C_5 carbonyl nitrate (ICN).

Scheme 2. Photooxidation Products (e.g., C_5 Nitrooxy Hydroxyepoxide (INHE)) of the Dominant β- and δ-C_5 Nitrooxy Hydroperoxide (INP)

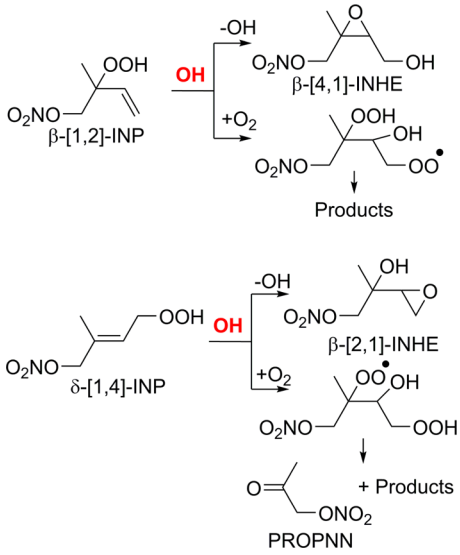

DOI: 10.1021/acs.jpca.5b06355
J. Phys. Chem. A 2015, 119, 10158−10171

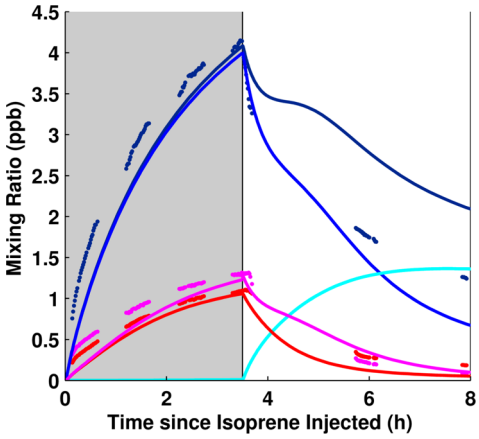

Figure 2. Major nitrates detected by the CIMS (markers, 1 min averages) and predicted by the kinetic mechanism explained in section S1 (solid lines) for experiment 8 including C_5 nitrooxy hydroperoxide (INP) + C_5 nitrooxy hydroxyepoxide (INHE) + C_5 dihydroxy nitrate (IDHN) [dark blue], C_5 hydroxy nitrate (IHN) [red], and C_5 carbonyl nitrate (ICN) [magenta]. The kinetic mechanism results for INP [blue] and INHE [cyan] are also presented separately for reference. The white background indicates when photooxidation occurred.

Table 3. Proposed Isomer Distribution for INP, ICN, and IHN, Including Uncertainties Due to Peak Integration and CIMS Sensitivity

	distribution of β-/δ-isomers		β- and δ-isomer distribution	
nitrate	isomer	percent	isomer	percent
C_5 nitrooxy hydroperoxide (INP)	β	30^{+9}_{-8}	β-[1,2]	88^{+4}_{-5}
			β-[4,3]	12^{+5}_{-4}
	δ	70^{+8}_{-9}	δ-[1,4]	84^{+7}_{-11}
			δ-[4,1]	16^{+11}_{-7}
C_5 carbonyl nitrate (ICN)	β	0	β-[1,2]	NA
			β-[4,3]	NA
	δ	100	δ-[1,4]	74^{+8}_{-9}
			δ-[4,1]	26^{+9}_{-8}
C_5 hydroxy nitrate (IHN)	β	20^{+7}_{-6}	β-[1,2]	0
			β-[4,3]	100
	δ	80^{+6}_{-7}	δ-[1,4]	86^{+6}_{-8}
			δ-[4,1]	14^{+8}_{-6}

had the lowest oxidant concentrations, which minimized second-generation chemistry. The first GC-ToF-CIMS chromatograph (49 min after the start of isoprene NO_3 oxidation) was used to calculate the fractions in Table 3 to limit the influence of wall loss and later generation chemistry.

Table 2. Molar Yield per Isoprene Reacted for Main Products Detected by the CIMS During Experiment 8 (at 2.5 h) Compared to Yields Reported Previously[a]

name	abbreviation	possible structure (single isomer shown)	CIMS *m/z* (-)	this study yield	literature yield	estimated vapor pressure (atm)[a]
C_5 nitrooxy hydroperoxide	INP	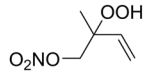	248			1.0×10^{-5}
C_5 nitrooxy hydroxyepoxide	INHE	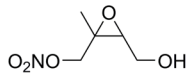	248	0.41 (combined)	0.123[15], 0.18[39] (combined)	7.6×10^{-6}
C_5 dihydroxy nitrate	IDHN	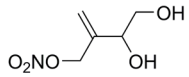	248			3.2×10^{-7}
C_5 carbonyl nitrate	ICN	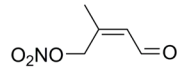	230	0.12	0.356[15], 0.51[39]	1.2×10^{-4}
C_5 hydroxy nitrate	IHN	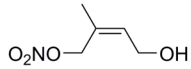	232	0.12	0.214[15], 0.27[39]	2.4×10^{-5}
C_5 dihydroxy carbonyl *	IDHC	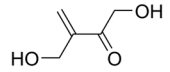	201	0.03	0.012[15]	1.5×10^{-6}
C_5 hydroxy hydroperoxy nitrate	IHPN	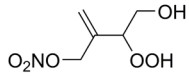	264	0.03	0.016[15]	3.0×10^{-8}
C_5 hydroxy carbonyl nitrate	IHCN	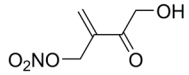	246	0.02	0.043[15]	3.6×10^{-6}
ROOR from INO_2 and hydroxy methyl peroxy or CIMS complex between INP and CH_2O *	INO2HM	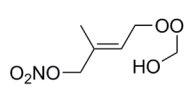	278	0.02		8.5×10^{-7}
Propanone nitrate	PROPNN	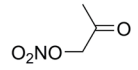	204	0.01		4.5×10^{-3}
Total Nitrates Detected				**0.76**	~0.80[12], 0.70 ±0.08[13], 0.65 ± 0.12[14], ~0.80[15]	

[a]Vapor pressure (atm, at 298 K) is estimated using the method EVAPORATION.[40] We note epoxides are not a functional group specifically within the scope of EVAPORATION. An asterisk denotes that the assignment of these compounds is tentative (see Supporting Information section S3.0); observed signal could be impacted by other compounds. References 12−15 and 39 are also cited in the body of the table.

DOI: 10.1021/acs.jpca.5b06355
J. Phys. Chem. A 2015, 119, 10158−10171

For INP, RO_2 + RO_2 chemistry clearly impacts the isomer distribution even in experiment 8 when RO_2 + RO_2 chemistry is limited (Figure 1). The first GC-ToF-CIMS results (39 min after photooxidation ended) for experiment 10 were used to determine the isomer distribution of INP. In this experiment RO_2 + RO_2 chemistry was much less prominent than experiment 8. For example, in experiments 7, 8, and 10 the ratio of β-INP compared to β-[4,3]-IHN, the IHN isomer produced from the RO_2 with the fastest expected RO_2 + RO_2 rate constant (section 4.2), was 2.5, 4.4, and 14.6. Experiment 10 contained a mixture of products from OH and NO_3 oxidation of isoprene, which made further use of this experiment difficult, but since INP forms only from isoprene and NO_3 oxidation, this experiment was optimal for determining these isomer ratios.

Synthetic standards are not available for most of the nitrates formed in this work, so the relative GC-ToF-CIMS elution times of synthetic standards from ISOPOOH/IEPOX[35] and hydroxy nitrates from isoprene OH oxidation[25] are used to assign the peaks to INP/INHE, ICN, and IHN. Uncertainties in Table 3 are derived from the uncertainty in integration (1 sigma) and uncertainty in the relative sensitivity between the isomers (20%). Peak assignments are shown in Figure S1 and Table S1, and the explanation for peak selection is discussed in section S2. Transmission through the GC-ToF-CIMS for all isomers reported in Table 3 was ~100%.

4.0. DISCUSSION

To analyze these experiments, we develop a kinetic mechanism for the isoprene−NO_3 reaction based on available recommended literature rates and branching ratios (see section S1 for details). The first-generation products explained in sections 4.2 and 4.3 including the isomer distributions of the significant nitrates reported in Table 3 are incorporated into the kinetic mechanism. For the most part, we use the literature rates and branching ratios without attempting to optimize the chemistry due to the complexity of the chamber mixture. Three primary oxidants are present (NO_3, O_3, and OH) within our experiments. The rates and products for reactions between these three oxidants and the isoprene nitrates produced via NO_3 oxidation are not well-known. As a result of the few constraints and large number of unknowns, a variety of solutions to the chemical mechanism can explain the observations equally well. Nevertheless, the kinetic mechanism developed here does inform our analysis and provide guidance for future studies.

We use the kinetic mechanism and the products detected to give insight on each step of isoprene oxidation by NO_3:

- NO_3 addition to isoprene and subsequent O_2 addition to form a nitrooxy peroxy radical (INO_2) (section 4.1)
- INO_2 reaction with either itself or another RO_2 (section 4.2), HO_2 (section 4.3), or NO/NO_3 to form nitrates, each with unique isomer distributions.
- The subsequent fate of these organic nitrates upon reaction with OH to form INHE, PROPNN, and other products (section 4.4), some of which (e.g., INHE) undergo reactive uptake to the aerosol phase (section 4.5).

4.1. Isoprene Nitrooxy Peroxy Radical (INO_2) Distribution. NO_3 adds to isoprene followed by O_2 addition to form isoprene nitrooxy peroxy radical (INO_2). There are few previous constraints[41−43] on the INO_2 distribution, but this distribution is important to understand as it determines the lifetime and subsequent photoproducts of the first-generation compounds. To determine the INO_2 distribution, we use the products of the INO_2 + HO_2 reaction (section 4.3, Table 5, column 2) and assume that each INO_2 reacts with HO_2 at the same rate, consistent with Jenkin and Hayman.[44] On the basis of this INO_2 distribution, NO_3 adds to the C_1 position of isoprene 7 ± 1 times faster than to the C_4 position. This range is on the high end of other experimental studies (3.5[41] and 5.1−7.4[42]) and a theoretical study (5.6).[43]

We find that δ-peroxy radicals are present in slightly higher quantities than β-peroxy radicals (~1.2:1), also consistent with previous studies. Skov et al.[41] proposed that the dominant product is [1,4]-ICN, but no quantitative data were provided. In a theoretical study, Zhao and Zhang[45] calculated that O_2 adds 1.15 times faster at the δ position. However, the ratio of the O_2 addition rates does not necessarily determine the δ/β distribution as Peeters et al.[46,47] have shown that the bond strength of the alkylperoxy radicals is sufficiently weak that, with a time constant of several seconds, the RO_2 will dissociate leading to a dynamic exchange between β- and δ-isomers. Zhao and Zhang[45] calculated that the energy differences (kcal mol^{-1}) between INO_2 and isoprene−NO_3 + O_2 are between 15.63−17.20 for β-INO_2 and 11.97−14.06 for δ-INO_2, suggesting that the reverse reaction will likely be important for INO_2.

Recently, a number of studies have highlighted the importance of RO_2 lifetime for isoprene oxidation by OH.[46,47] The lifetime influences the isomer distribution, which, in turn, influences later generation products and likely SOA formation. We suspect that the RO_2 lifetime is also important for isoprene oxidation by NO_3. According to the kinetic mechanism developed here, the INO_2 lifetime at the beginning of experiments 5, 6, 8, and 10 was ~7, ~ 10, ~ 30, and ~20 s, respectively. However, across all experiments the estimated INO_2 lifetime increased with time. For example, the INO_2 overall lifetime prior to photooxidation in experiment 8 was estimated to be ~80 s. Reaction of INO_2 + NO_2 was not included in the INO_2 lifetime calculation because the peroxynitrate that forms is believed to quickly decompose back to INO_2 and NO_2 without altering the initial isomer distribution. The INO_2 distribution determined in this work is for an RO_2 lifetime of ~30 s as most of the distribution is based on the INP isomer fractions measured during experiment 10, and the average lifetime between the start of NO_3 oxidation and the first GC collection time is ~30 s. An RO_2 lifetime of ~30 s may be representative of that at night in the urban atmosphere (~50 s), but the lifetime for rural conditions may be much longer (~200 s), assuming HO_2 is 5 ppt and RO_2 is 20 ppt[48] for both conditions, and NO_3 is 1 ppt in rural[24] and 300 ppt in urban[48] conditions with the rate constants assumed in the kinetic mechanism.

Our data suggest that for an INO_2 lifetime of ~30 s, the δ-INO_2 concentration is 1.1−1.2 times more abundant than the β-INO_2 isomer. On the basis of theoretical calculations, Peeters et al.[47] calculated that for OH-initiated oxidation of isoprene at 295 K the β-isomer would, in contrast, be nearly ~30 times higher than the δ-isomer for RO_2 at a similar lifetime. This suggests that the alkylperoxy radical kinetics and thermodynamics are quite different for NO_3 derived peroxy radicals.

4.2. RO_2 + RO_2 Reaction Rates. As shown in Scheme 1, INO_2 can react with itself or another RO_2 radical to form IHN and ICN or two alkoxy radicals (INO). In order to constrain

DOI: 10.1021/acs.jpca.5b06355
J. Phys. Chem. A 2015, 119, 10158−10171

Table 4. Isomer Specific IHO_2 + IHO_2 Rate Constants Compared to Estimated INO_2 + INO_2 Rate Constants

isomer	RO_2 + RO_2 product distribution	normalized RO_2 + RO_2 product distribution[a]	$k_{IHO_2+IHO_2}$ (cm^3 $molecule^{-1}$ s^{-1})[49]	estimated $k_{INO_2+INO_2}$ (cm^3 $molecule^{-1}$ s^{-1})
β-[1,2]	1.5×10^{-3}	$(3.5–3.6) \times 10^{-3}$	6.92×10^{-14}	1.8×10^{-14}
β-[4,3]	0.12	2.2–4.6	5.74×10^{-12}	$(1.1–2.3) \times 10^{-11}$
δ-[1,4]	0.73	1.6	3.90×10^{-12}	$(7.9–8.2) \times 10^{-12}$
δ-[4,1]	0.15	1.7	2.77×10^{-12}	$(8.3–8.6) \times 10^{-12}$

[a]The normalized RO_2 + RO_2 product distribution is the RO_2 + RO_2 product distribution (column 2) divided by the INO_2 distribution estimated by the INO_2 + HO_2 products (Table 5, column 2).

the MVK and MACR yields from the RO_2 + HO_2 pathway, the yields of MVK and MACR from the RO_2 + RO_2 pathway need to be approximated. In experiment 8, IHN, ICN, and INO predominantly come from RO_2 + RO_2 reactions because NO and NO_3 levels are so low (Figure 1). The IHN and ICN isomer distributions can give insight into the RO_2 + RO_2 self-reaction rates of INO_2. The alkoxy radical can either react with O_2 to form HO_2 and ICN or undergo a [1,5]-H-shift (Scheme S3). We detect the same products Kwan et al.[15] proposed formed from the [1,5]-H-shift of the *trans*-[1,4]-INO. Additionally, recent studies for similar alkoxy radicals[47] suggest that the *trans*- and *cis*-[1,4]-INO may interconvert rapidly (see section S3.1 for more details). Because of this, the ICN distribution favors the [4,1]-isomer more than the INP and IHN distribution (Table 3). The distribution of IHN, ICN, and the [1,5]-H-shift products are shown in Table 4, column 2. To calculate this distribution, we assumed that for every [1,2]-IHN or [4,3]-IHN detected there is a corresponding MVK or MACR formed. This product distribution is included in the kinetic mechanism.

MCM v3.2[50] recommends a single rate coefficient of 1.3×10^{-12} cm^3 $molecule^{-1}$ s^{-1} for all isomers of INO_2 + INO_2. However, for isoprene RO_2 species from OH oxidation (IHO_2), MCM v 3.2[50] recommends isomer specific rates based on a study done by Jenkin et al.[49] (Table 4, column 4). To our knowledge, there are no direct studies on how nitrate groups influence RO_2 + RO_2 rates. β-Chloro, β-bromo, and β-hydroxy functional groups seem, however, to similarly increase the RO_2 + RO_2 rates.[44,51,52] Similar to nitrooxy, all of these substituents are electron-withdrawing, so *a priori* we would expect that the RO_2 kinetics would follow a similar pattern.

As shown in Figure 2, the kinetic mechanism best captures the formation rate of IHN when one uses a general rate constant for INO_2 + INO_2 of $\sim 5 \times 10^{-12}$ cm^3 $molecule^{-1}$ s^{-1}. A general rate constant of $\sim 3 \times 10^{-12}$ cm^3 $molecule^{-1}$ s^{-1} produces enough IHN in the kinetic mechanism to be within the uncertainty of the ToF-CIMS results. This general INO_2 + INO_2 rate constant is much larger than that included in MCM v3.2,[50] CMAQ,[20] or GEOS-CHEM.[53] The present study, however, does not provide ideal conditions to measure the RO_2 + RO_2 reaction rates as CH_2O and HO_2 will react reversibly to form the hydroxy methylperoxy radical (HMP) and the equilibrium constant for this reaction is not well-constrained (IUPAC[11]). Additionally, it is possible that the HMP + HMP reaction rate constant is faster than that recommended by IUPAC. Thus, although the high general RO_2 + RO_2 rate constant used in this work is necessary to constrain the products from the RO_2 + RO_2 pathway, it is possible that this rate constant leads to a better fit of the data (Figure 2) merely because of uncertainties in HMP formation and subsequent reaction (section S1.2). It is recommended that a separate study be carried out to independently measure the general INO_2 + INO_2 rate constant.

To estimate the isomer-specific self-reaction rates, we normalize by the INO_2 distribution fractions based on the INO_2 + HO_2 products (Table 5, column 2). Although studies have confirmed that RO_2 + HO_2 rate constants are influenced by carbon number,[50] it appears that the type of peroxy radical (i.e., primary, secondary, or tertiary) does not substantially impact the RO_2 + HO_2 reaction rate constants.[44] Provided that the INO_2 + HO_2 rate constants are not isomer dependent, the ratio of the RO_2 + RO_2 products to the INO_2 + HO_2 products represents the relative RO_2 + RO_2 reaction rate distribution between the isomers (normalized RO_2 + RO_2 product distribution, Table 4, column 3). The isomer specific RO_2 + RO_2 reaction rate constants were estimated by combining the generalized reaction rate constant ($\sim 5 \times 10^{-12}$ cm^3 $molecule^{-1}$ s^{-1}) based on IHN formation with the normalized RO_2 + RO_2 product distributions based largely on the GC-ToF-CIMS results. The β-[4,3]-IHO_2 self-reaction rate constant is the largest (Table 4) consistent with the measured isomer dependent IHO_2 + IHO_2 rate constants.[49]

Table 5. Isomer Dependent Product Distribution of INO_2 + HO_2

INO_2	fraction	products	yield
β-[1,2]-	0.42	OH + MVK + CH_2O + NO_2	0.53
		β-[1,2]-INP	0.47
β-[4,3]-	0.03–0.06	OH + MACR + CH_2O + NO_2	0–0.53
		β-[4,3]-INP	0.47–1
δ-[1,4]-	0.44–0.46	δ-[1,4]-INP	1
δ-[4,1]-	0.08–0.09	δ-[4,1]-INP	1

4.3. INO_2 + HO_2 Reaction Products. Hydroperoxides have typically been assumed to be the dominant product of the RO_2 + HO_2 reaction pathway. Recent studies of acetylperoxy radical[54−58] and α-carbonyl peroxy radical[37,55,59,60] reactions with HO_2 have found, however, that a variety of other products can form (R9–R11):

$$RO_2 + HO_2 \rightarrow ROOH + O_2 \quad \text{(R9)}$$

$$RO_2 + HO_2 \rightarrow ROH + O_3 \quad \text{(R10)}$$

$$RO_2 + HO_2 \rightarrow RO + OH + O_2 \quad \text{(R11)}$$

Rollins et al.[13] and Kwan et al.[15] proposed that the INO_2 + HO_2 reaction produces OH as well as INP. Using the formation of isoprene OH oxidation products (e.g., hydroxy hydroperoxide (ISOPOOH)) as tracers for OH chemistry, Kwan et al.[15] suggested that 38–58% of the total INO_2 + HO_2 reactions produce OH via channel R11. Hou et al.[61] and Hou and Wang[62] have proposed a different reaction pathway (R12), in which OH, HO_2, and R′CHO form:

DOI: 10.1021/acs.jpca.5b06355
J. Phys. Chem. A 2015, 119, 10158–10171

Scheme 3. Dominant Decomposition Products from the Reaction of INP, IHN, and ICN with OH

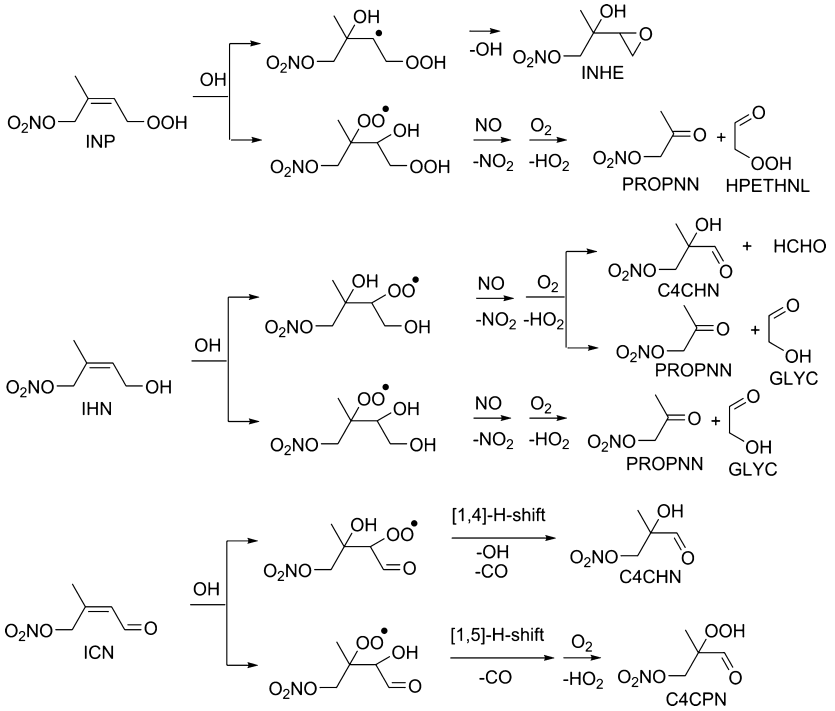

For brevity, reactions for only the dominant isomer ([1,4]) and only major products are shown. See section S1.4 for more details on additional products, branching ratios, and rates used in the kinetic mechanism. Acronyms not yet defined are glycolaldehyde (GLYC) and hydroperoxyethanal (HPETHNL).

$$RO_2 + HO_2 \rightarrow OH + HO_2 + R'CHO \quad (R12)$$

R12 has also been suggested to be important in the reactions of RO_2 produced from MVK + OH + O_2 with HO_2 radicals.[37]

The β-isomers, [1,2]-INO_2 and [4,3]-INO_2, may react with HO_2 to produce OH and MVK or MACR. The MVK and MACR yield from the INO_2 + HO_2 pathway is inferred by subtracting all known sources of MVK and MACR (as predicted by the kinetic simulation) from the observations and assuming the remainder arises from the INO_2 + HO_2 pathway. The overall MVK (12.3%) and MACR (4.8%) yields (relative to isoprene consumed) from experiment 6 were used, as experiments 1−5 have an unknown GC-FID interference following the subsequent injections of O_3. In experiment 6, we were able to quantify MVK and MACR after all O_3 had reacted away. Additionally, a cold trap (−40 °C) was used upstream of the GC-FID to remove interferences from hydroperoxides/epoxides.[26,27]

The yield of MVK from RO_2 + HO_2 compared to RO_2 + RO_2 reactions is expected to be quite high given that the β-[1,2]-INO_2 + RO_2 reaction rate constant is expected to be small (section 4.2). Conversely, MACR yields from the RO_2 + HO_2 pathway will be difficult to constrain given that the β-[4,3]-INO_2 + RO_2 reaction rate constant is quite high. A general RO_2 + HO_2 branching ratio of 0.22 for MVK best matches with the present experimental data, but the kinetic mechanism over-predicts MACR even without an additional yield from the RO_2 + HO_2 pathway. This is likely a result of the assumption that for every [4,3]-IHN detected there is a corresponding MACR formed. The exact distribution of products from RO_2 + RO_2 self- and cross-reactions is uncertain. We calculate the isomer dependent product distribution of INO_2 + HO_2 based on the isomer distribution of INP (Table 3) and the kinetic mechanism determined MVK yields. For the MACR yield from β-[4,3]-INO_2 + HO_2 we report a range from 0 to the yield of MVK from β-[1,2]-INO_2 + HO_2 as we expect less substituted nitrooxy peroxy radicals to produce less OH than their tertiary counterparts.[59]

The OH yield has only been measured for a small subset of alkylperoxy radicals. The HO_x recycling implied from the product distributions of β-[1,2]-INO_2 agrees with available data. For example, Hasson et al.[59] found that the secondary RO_2 $CH_3C(O)CH(O_2)CH_3$ produces 0.58 OH and Praske et al.[37] found that the secondary RO_2 $CH_3C(O)CH(O_2)CH_2OH$ produces 0.66 OH from reaction with HO_2.

When an OH yield of 0.22−0.25 (i.e., coproduct of MVK and MACR) is incorporated into the kinetic mechanism for the RO_2 + HO_2 reaction, ISOPOOH formation is underpredicted prior to photooxidation for experiments 3−5 by ∼29−34% (not shown), which may indicate "missing" OH in the experiment. However, the agreement is within the uncertainty of the triple-CIMS measurements (±35%, see section S3), and the yield of ISOPOOH will be dependent on the RO_2 + RO_2 reaction rates used in the kinetic mechanism, which are not well constrained. MS/MS CIMS and the GC-ToF-CIMS verify that the initial chemistry produces only ISOPOOH, so formation of IEPOX, an isobaric compound, is not causing this discrepancy.

Furthermore, we confirm this potentially "missing" OH is not likely from the reaction of δ-INO_2 + HO_2 + O_2 → OH + HO_2 + ICN. The ratios of INP:IHN and ICN:IHN are 2.4 and 1.5, respectively, for experiment 7 while for experiment 8 these ratios are 3.2 and 1.2, respectively. Given that RO_2 + HO_2 reactions are more dominant in experiment 8 (Figure 1), if ICN is formed from δ-INO_2 + HO_2 reactions, both the INP:IHN and ICN:IHN ratios should increase, but only the INP:IHN

DOI: 10.1021/acs.jpca.5b06355
J. Phys. Chem. A 2015, 119, 10158−10171

ratio increased from experiment 7 to 8. This strongly suggests that ICN is not a major product of the RO_2 + HO_2 pathway.

Thus, evidence suggests that the general RO_2 + HO_2 reaction products are 0.22 MVK, 0−0.03 MACR, 0.22−0.25 OH, 0.22−0.25 CH_2O, 0.22−0.25 NO_2, and 0.75−0.78 INP. Assuming the midpoint of the MACR range forms, the kinetic mechanism matches experimental results reasonably well (Figure 2).

4.4. Photooxidation of First-Generation Nitrates. Photooxidation was initiated after generating the first-generation nitrates to monitor their reaction with OH (Scheme 3). This chemistry is relevant in regions where NO_3 reacts with isoprene during the day (under clouds and within forest canopies) or at sunrise when NO_3 and OH chemistry regimes overlap.

4.4.1. INHE Formation. We propose that INP reacts with OH to form INHE (Scheme 2). INP and INHE are isobaric compounds. For naming INHE isomers, the first number corresponds to the hydroxy group, and the second number to the nitrate group.

C_5 dihydroxy nitrate (IDHN) is also isobaric with INP and INHE. IDHN was first proposed by Kwan et al.[15] along with C_5 hydroxy carbonyl nitrate (IHCN) and C_5 hydroxy hydroperoxy nitrate (IHPN) to be a product of the 1,5 H-shift of *trans*-[1,4]-INO (Scheme S3). Unfortunately, we suspect δ-INHE and IDHN coelute in the GC-ToF CIMS so individual quantification was not possible (see section S2 for more details on peak assignments). When photooxidation was started, IHCN, a coproduct with IDHN from RO_2 + RO_2 reactions, increased initially but then leveled off, while the peak containing δ-INHE and IDHN kept rising (Figure S2). We subtract the IHCN signal from the δ-INHE and IDHN signal, and assume the remaining signal is δ-INHE (Figure 3).

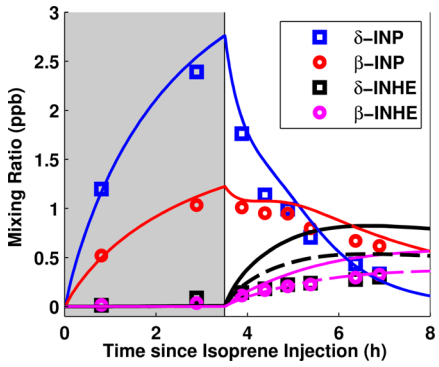

Figure 3. GC-ToF-CIMS data (markers) and kinetic mechanism results (lines) for δ- and β-isomers of INP and INHE. δ-INP GC-ToF-CIMS results are corrected for the low transmission rate through the 4m column (see section S2.0). Solid lines indicate the base case of the mechanism, and dashed lines are results from reducing the INHE yield from INP + OH in the kinetic mechanism.

Although this correction is sensitive to yields of these 1,5 H-shift products, IDHN should be less than IHCN, resulting in overcorrection; δ-INHE can be observed to be clearly formed when photooxidation started after this correction (Figure 3). The peaks for the remaining products, δ-INP, β-INP, and β-INHE, are distinct, and no correction is needed.

Figure 3 suggests that the kinetic mechanism may over-predict INHE formation, but this depends on many factors including, but not limited to, CIMS calibration factors, the O_3 and OH reaction rates of β-INP, and δ-INP, transmission through the 4 m GC column, the loss rate of INHE itself with OH and walls of the chamber, and the amount of IDHN formed. It is possible INHE has a higher wall loss than INP due to nitric acid acidifying the chamber walls. In the kinetic mechanism, the INHE yields from the reaction of δ-INP and β-INP with OH are assumed to be 0.37 and 0.78, respectively, based on the location of OH addition to standards similar to δ-INP and β-INP[36,63] and the assumption that if the nascent alkyl radical is β to the hydroperoxide, INHE forms with unity yield. Because of the presence of the nitrooxy group, the lifetime of the alkyl radical before elimination of OH and formation of the epoxide may be longer than for ISOPOOH. If so, a larger fraction of the alkyl radicals may add O_2 precluding INHE formation.

The yield of non-IEPOX products from OH addition to [1,2]-ISOPOOH and [4,3]-ISOPOOH has been measured to be ∼0.13.[63] Some of these products are likely from O_2 addition prior to formation of IEPOX especially for [4,3]-ISOPOOH where OH is expected to add to the internal carbon minimally if OH addition is similar to MACR (0.035 for internal addition).[64] For the dashed line, in Figure 3, a reduction of the δ- and β-INHE yield in the kinetic mechanism by 36% for both isomers leads to a better match of β-INHE with experimental results. Given that δ-INHE coelutes with IDHN, we do not use the experimental results to optimize the yield of δ-INHE, but it appears that a reduction >36% is necessary. Thus, results suggest that an INHE yield from the reaction of δ-INP and β-INP with OH should be <0.24 and ∼0.50, respectively. Figure 4 demonstrates that with this change PROPNN still reasonably aligns with experimental results.

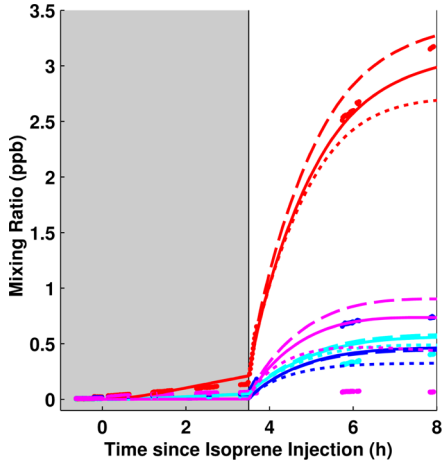

Figure 4. Experimental results (markers, 1 min averages) and kinetic mechanism results (lines) for propanone nitrate (red), ethanal nitrate (cyan), C_4 carbonyl hydroxynitrate (blue), and C_4 carbonyl hydroperoxynitrate (magenta) from experiment 8. Solid lines are for the base case, dashed lines are for revised IHNE yield (section 4.4.1), and dotted lines are for the revised photolysis reactions (section 4.4.2).

4.4.2. Decomposition Products. Figure 4 and Scheme 3 show the primary nitrate decomposition products formed when INP, ICN, and IHN are photooxidized during experiment 8. Propanone nitrate (PROPNN) is observed with high yield. This is expected given that [1,4]-INO_2 is likely the dominant peroxy radical formed upon reaction of isoprene with OH. This chemistry has important atmospheric consequences because PROPNN has a fairly long photochemical lifetime in the atmosphere (∼7.1 h including loss due to OH and

DOI: 10.1021/acs.jpca.5b06355
J. Phys. Chem. A 2015, 119, 10158−10171

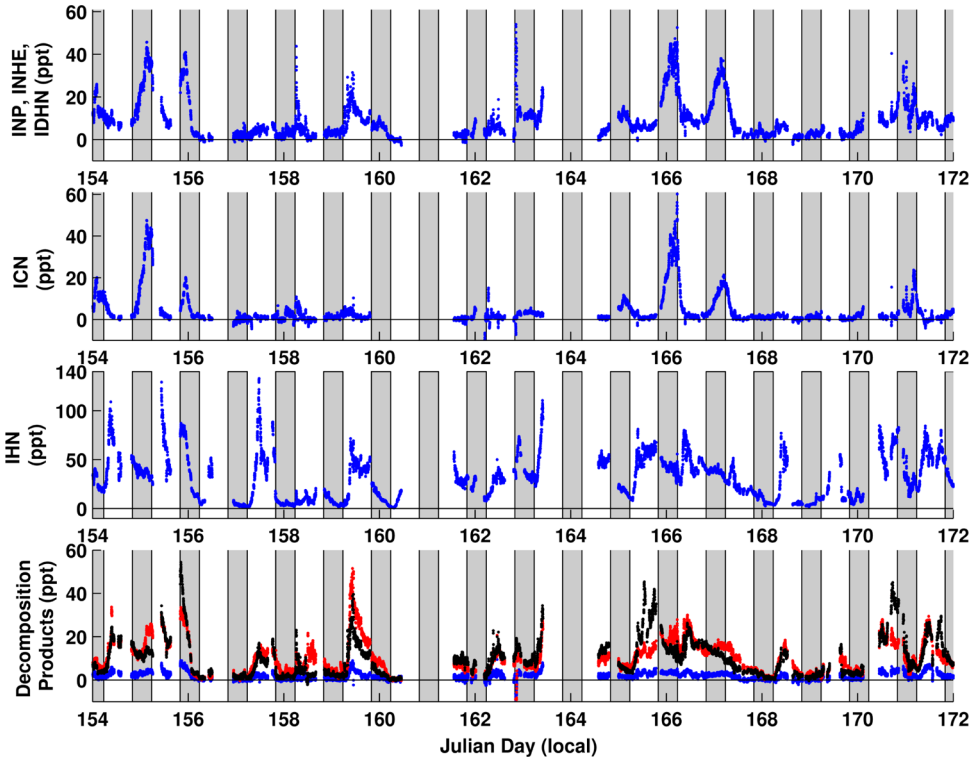

Figure 5. C_5 nitrooxy hydroperoxide (INP) + C_5 nitrooxy hydroxyepoxide (INHE) + C_5 dihydroxy nitrate (IDHN) [1st panel]; C_5 carbonyl nitrate (ICN) [2nd panel], C_5 hydroxy nitrate (IHN) [3rd panel], and primary decomposition products (ethanal nitrate (ETHLN) [blue], propanone nitrate (PROPNN) [red], and C_4 carbonyl hydroxynitrate (C4CHN) [black]) for several weeks during the SOAS 2013 field campaign. The shaded area represents nighttime. No fragmentation correction was applied for INP (section 3.0), which may bias results low.

photolysis),[65] although its dry deposition velocity is significant (~2 cm s^{-1}).[66]

ICN, IHN, and INP are assumed to react with OH and O_3 similarly to the only standards that have been measured, [1,4N]-IHN and [4,3N]-IHN (see Scheme 3 and section S1.4 for more details).[38,67] The kinetic mechanism overpredicts ethanal nitrate (ETHLN) and C_4 carbonyl hydroperoxynitrate (C4CPN), but underpredicts C_4 carbonyl hydroxynitrate (C4CHN) (Figure 4). C4CPN is assumed to form from the peroxy radical, formed from ICN reacting with OH, undergoing a [1,5]-H shift (Scheme 3 and S2) similar to the chemistry proposed by Crounse et al. for MACR.[64] C4CPN is barely detected, but we expect this [1,5]-H-shift to be quite fast because the [1,4]-H-shift for MACR[64] occurs at 0.5 s^{-1}, and the [1,5]-H shift should be much faster. Possibly, the [1,5]-H shift leads to further decomposition forming PROPNN instead of C4CPN. Additionally, C4CPN might fragment while being ionized by CF_3O^-. For example, β-[1,2]-INP fragments by ~20% (this work) and 3-hydroperoxy-4-hydroxybutan-2-one has been identified to fragment by 78%.[37] Owing to the number of compounds present during photooxidation it is difficult to determine the fragmentation pattern of C4CPN. In the kinetic mechanism, C4CPN is assumed to photolyze to MGLYX + OH + NO_2 + CH_2O. No instrumentation was available to detect MGLYX to confirm that this process occurred.

We use the kinetic mechanism to test the extent to which loss due to photolysis can explain the under-prediction of C4CPN. Theoretical[68] and experimental[69] studies have found that hydroperoxyenals photolyze with a quantum yield of ~1, and Muller et al.[65] proposed that many of the α-nitrooxy aldehydes and ketones derived from isoprene also photolyze with a quantum yield of ~1. We revised the default MCM v3.2[50] quantum yield for PROPNN and ETHLN from 0.22 to 1, and for ICN from 0.00195 to 1. Although Wolfe et al.[69] only verified that hydroperoxyenals photolyze with a quantum yield of ~1, we also assume that a similar effect occurs for α-hydroperoxy carbonyls (e.g., C4CPN). As shown in Figure 4 (dotted lines), adding photolysis losses to the base case of the kinetic mechanism lowers the predicted amount of nitrates formed, but not outside of expected uncertainty (instrumental and kinetic mechanism assumptions). Even after increasing the rate of photolysis, C4CPN is still overpredicted by the kinetic mechanism, suggesting that the absorption cross sections could be larger than estimated due to the combined presence of a carbonyl, hydroperoxy, and nitrate group. Alternatively, the low signal may arise because either C4CPN does not form or C4CPN is fragmented during ionization.

Beyond the first-generation products, differences between the kinetic simulations and the experimental data cannot be securely tied to any particular uncertainty in the mechanism, owing to the complexity of the system. Nevertheless, the kinetic mechanism developed here suggests that using current understanding of how OH reacts with isoprene nitrates enables at least qualitatively correct simulations of the formation of the major nitrate decomposition products.

4.5. INHE Uptake onto Aerosols. INHE, similar to IEPOX,[33,70] efficiently undergoes reactive uptake to highly acidified aerosol (section S4 of the Supporting Information). The INHE/IDHN-derived fragments in the AMS are identical to IEPOX ($C_4H_5^+$, $C_5H_6O^+$, $C_3H_7O_2^+$, and $C_5H_8O_2^+$)[71] for highly acidic seed (likely due to the hydrolysis of the nitrate group). Thus, in the atmosphere under acidic conditions, INHE and IDHN likely add to the AMS tracer fragments that are generally assigned solely to IEPOX.

DOI: 10.1021/acs.jpca.5b06355
J. Phys. Chem. A 2015, 119, 10158−10171

We would expect INHE, like IEPOX,[31] to undergo reactive uptake to aqueous ammonium sulfate aerosol. There is an increase in the total organic mass measured by the AMS for hydrated ammonium sulfate aerosol compared to dry ammonium sulfate aerosol, but our results are inconclusive as this could be due to INHE or other nitrates partitioning. From this work we find that a large fraction of the nitrates produced from NO_3 oxidation are in the δ-state (Table 3). If other δ-nitrates hydrolyze as quickly as δ-[1,4N]-IHN (neutral hydrolysis lifetime of 2.46 min),[67] then the nitrates produced from NO_3 oxidation might be an important sink for NO_3 in humid locations. Further chamber studies run at a full range of relative humidities using synthetic standards of INHE and other nitrates are needed to better understand the influence isoprene NO_3 oxidation has on SOA formed under humid conditions.

5.0. ATMOSPHERIC RELEVANCE

During the SOAS field campaign (June to July 2013 in Brent, AL), products from NO_3 oxidation of isoprene were detected in the ambient atmosphere (Figure 5). Consistent with the chemistry described here, ICN and INP/IDHN/INHE generally exhibit a nighttime peaking diurnal pattern, while IHN has a less clear diurnal pattern because it is produced from both the OH- and NO_3-initiated oxidation of isoprene. Additionally, when ICN and INP/IDHN/INHE formed at night, their combined magnitude was similar to the amount of IHN formed during the day. INP/IDHN/INHE and ICN were observed in similar amounts, highlighting the importance of RO_2 + HO_2 chemistry. ICN and INP/IDHN/INHE concentrations at night were quite variable during the campaign, likely reflecting changes in atmospheric conditions (O_3, NO_2, temperature, isoprene).

On several days when ICN and INP/IDHN/INHE were detected at night, the main decomposition nitrates (PROPNN, ETHLN, and C4CHN) increased after sunrise, but this effect was not seen for all instances when ICN and INP/IDHN/INHE formed at night. It is difficult to attribute the formation of PROPNN, ETHLN, and C4CHN solely to chemical production given the large change in boundary layer dynamics forced by the increased surface heating. On some days, PROPNN, ETHLN, and/or C4CHN increased at sunrise even when ICN and INP/IDHN/INHE were not detected the night before. This does not necessarily suggest these products cannot be used as tracers for the nitrates derived from isoprene + NO_3 because only measurements in the planetary boundary layer were made during SOAS by Caltech. It is possible that ICN and INP/IDHN/INHE were produced in the residual layer at night, and in the morning the photooxidation products were detected at the surface due to the rapid mixing that occurs at sunrise. Field studies measuring the formation of compounds in both the planetary boundary layer and residual layer at sunrise would be useful to better understand how PROPNN, ETHLN, and C4CHN form in the atmosphere.

6.0. CONCLUSIONS

In this work, the alkylperoxy radical isomer distribution and product yields in the reaction of NO_3 with isoprene were determined at an RO_2 lifetime of ~30 s. δ-Nitrooxy alkylperoxy radicals are slightly more abundant than their β counterparts suggesting the alkylperoxy radical kinetics and thermodynamics are quite different for NO_3 vs OH derived peroxy radicals. The nitrate yield (i.e., isoprene nitrooxy hydroperoxide (INP) yield) from the RO_2 + HO_2 pathway is high (~0.78). Additionally, we find an OH yield (~0.22) from the INO_2 + HO_2 pathway. Updating the products for the INO_2 + HO_2 reaction into mechanisms will lead to more accurate predictions of atmospheric NO_x and O_3 levels.

A large fraction of the nitrates produced from the NO_3-initiated oxidation of isoprene are δ-isomers. Since δ-[1,4N]-IHN has been shown to hydrolyze quickly in neutral liquid water,[67] isoprene NO_3 oxidation could be important as a terminal sink for NO_x in humid locations.

Because the lifetimes of isoprene nitrates with respect to oxidation by ozone (O_3) and NO_3 are quite long, most of the nitrates formed from isoprene oxidation by NO_3 will remain in the atmosphere until sunrise when OH begins to form. Qualitatively, the decomposition products from the photooxidation of the major NO_3 first-generation nitrates can be predicted using the isomer distributions determined by this study and current literature understanding, but to make further progress, synthetic standards are needed. Because δ-[1,4]-nitrates are the dominant products, PROPNN is the major nitrate decomposition product.

Results from these chamber experiments suggest that OH will react with INP to form INHE, a newly identified product, which appears to have similar heterogeneous fates to IEPOX. INHE has a lower yield from INP than IEPOX has from ISOPOOH and is limited by the amount of INP remaining in the atmosphere at sunrise, so the impact of INHE on SOA formation is likely to be far less than that of IEPOX. Future studies measuring the INHE reaction rate with OH and its uptake potential to hydrated aerosol (specifically chamber studies using a synthetic standard of INHE and higher relative humidity) will be useful to elucidate the full impact of INHE on SOA.

■ ASSOCIATED CONTENT

Supporting Information

The Supporting Information is available free of charge on the ACS Publications website at DOI: 10.1021/acs.jpca.5b06355.

Explanation of kinetic mechanism development (section S1), explanation of peak assignments for GC-ToF CIMS (section S2), analysis of gas-phase products from NO_3 oxidation (section S3), detailed analysis of the uptake of INHE and other products into aerosol seed (section S4), and sensitivity factors used for the CIMS and all reactions and rate constants used in the kinetic mechanism (Appendix) (PDF)

■ AUTHOR INFORMATION

Corresponding Authors

*(R.H.S.) E-mail: rschwant@caltech.edu.

*(P.O.W.) E-mail: wennberg@gps.caltech.edu.

Notes

The authors declare no competing financial interest.

■ ACKNOWLEDGMENTS

The authors thank the National Science Foundation (AGS-1240604) and the Electric Power Research Institute for their support of this work. TBN acknowledges support from NSF PRF award AGS-1331360. Development of the GC-ToF-CIMS is supported by an award from the National Science Foundation's Major Research Instrumentation Program (AGS-1428482).

DOI: 10.1021/acs.jpca.5b06355
J. Phys. Chem. A 2015, 119, 10158−10171

REFERENCES

(1) Monson, R. K.; Fall, R. Isoprene Emission from Aspen Leaves: Influence of Environment and Relation to Photosynthesis and Photorespiration. *Plant Physiol.* **1989**, *90*, 267−274.

(2) Loreto, F.; Sharkey, T. D. A Gas-Exchange Study of Photosynthesis and Isoprene Emission in Quercus Rubra L. *Planta* **1990**, *182*, 523−531.

(3) Starn, T. K.; Shepson, P. B.; Bertman, S. B.; Riemer, D. D.; Zika, R. G.; Olszyna, K. Nighttime Isoprene Chemistry at an Urban-Impacted Forest Site. *J. Geophys. Res.* **1998**, *103*, 22437−22447.

(4) Stroud, C. A.; Roberts, J. M.; Williams, E. J.; Hereid, D.; Angevine, W. M.; Fehsenfeld, F. C.; Wisthaler, A.; Hansel, A.; Martinez-Harder, M.; Harder, H.; et al. Nighttime Isoprene Trends at an Urban Forested Site during the 1999 Southern Oxidant Study. *J. Geophys. Res.* **2002**, *107*, 7-1−7-14.

(5) Steinbacher, M.; Dommen, J.; Ordonez, C.; Reimann, S.; Gruebler, F. C.; Staehelin, J.; Andreani-Aksoyoglu, S.; Prevot, A. S. H. Volatile Organic Compounds in the Po Basin. Part B: Biogenic VOCs. *J. Atmos. Chem.* **2005**, *51*, 293−315.

(6) Warneke, C.; de Gouw, J. A.; Goldan, P. D.; Kuster, W. C.; Williams, E. J.; Lerner, B. M.; Jakoubek, R.; Brown, S. S.; Stark, H.; Aldener, M.; et al. Comparison of Daytime and Nighttime Oxidation of Biogenic and Anthropogenic VOCs along the New England Coast in Summer during New England Air Quality Study 2002. *J. Geophys. Res.* **2004**, *109*, D10309.

(7) Brown, S. S.; DeGouw, J. A.; Warneke, C.; Ryerson, T. B.; Dube, W. P.; Atlas, E.; Weber, R. J.; Peltier, R. E.; Neuman, J. A.; Roberts, J. M.; et al. Nocturnal Isoprene Oxidation over the Northeast United States in Summer and Its Impact on Reactive Nitrogen Partitioning and Secondary Organic Aerosol. *Atmos. Chem. Phys.* **2009**, *9*, 3027−3042.

(8) Beaver, M. R.; St. Clair, J. M.; Paulot, F.; Spencer, K. M.; Crounse, J. D.; LaFranchi, B. W.; Min, K. E.; Pusede, S. E.; Wooldridge, P. J.; Schade, G. W.; et al. Importance of Biogenic Precursors to the Budget of Organic Nitrates: Observations of Multifunctional Organic Nitrates by CIMS and TD-LIF during BEARPEX 2009. *Atmos. Chem. Phys.* **2012**, *12*, 5773−5785.

(9) Brown, S. S.; Ryerson, T. B.; Wollny, A. G.; Brock, C. A.; Peltier, R.; Sullivan, A. P.; Weber, R. J.; Dubé, W. P.; Trainer, M.; Meagher, J. F.; et al. Variability in Nocturnal Nitrogen Oxide Processing and Its Role in Regional Air Quality. *Science* **2006**, *311*, 67−70.

(10) Sander, S. P.; Abbatt, J.; Barker, J. R.; Burkholder, J. B.; Friedl, R. R.; Golden, D. M.; Huie, R. E.; Kolb, C. E.; Kurylo, M. J.; Moortgat, G. K., et al. *Chemical Kinetics and Photochemical Data for Use in Atmospheric Studies, Evaluation No. 17*; JPL Publication 10−6: Jet Propulsion Laboratory: Pasadena, CA, 2011.

(11) Atkinson, R.; Baulch, D. L.; Cox, R. A.; Crowley, J. N.; Hampson, R. F.; Hynes, R. G.; Jenkin, M. E.; Rossi, M. J.; Troe, J.; Subcommittee, I. Evaluated Kinetic and Photochemical Data for Atmospheric Chemistry: Volume II − Gas Phase Reactions of Organic Species. *Atmos. Chem. Phys.* **2006**, *6*, 3625−4055.

(12) Barnes, I.; Bastian, V.; Becker, K. H.; Tong, Z. Kinetics and Products of the Reactions of NO_3 with Monoalkenes, Dialkenes, and Monoterpenes. *J. Phys. Chem.* **1990**, *94*, 2413−2419.

(13) Rollins, A. W.; Kiendler-Scharr, A.; Fry, J. L.; Brauers, T.; Brown, S. S.; Dorn, H.; Dube, W. P.; Fuchs, H.; Mensah, A.; Mentel, T. F.; et al. Isoprene Oxidation by Nitrate Radical: Alkyl Nitrate and Secondary Organic Aerosol Yields. *Atmos. Chem. Phys.* **2009**, *9*, 6685−6703.

(14) Perring, A. E.; Wisthaler, A.; Graus, M.; Wooldridge, P. J.; Lockwood, A. L.; Mielke, L. H.; Shepson, P. B.; Hansel, A.; Cohen, R. C. A Product Study of the Isoprene + NO_3 Reaction. *Atmos. Chem. Phys.* **2009**, *9*, 4945−4956.

(15) Kwan, A. J.; Chan, A. W. H.; Ng, N. L.; Kjaergaard, H. G.; Seinfeld, J. H.; Wennberg, P. O. Peroxy Radical Chemistry and OH Radical Production during the NO_3-Initiated Oxidation of Isoprene. *Atmos. Chem. Phys.* **2012**, *12*, 7499−7515.

(16) Sprengnether, M.; Demerjian, K. L.; Donahue, N. M.; Anderson, J. G. Product Analysis of the OH Oxidation of Isoprene and 1,3-Butadiene in the Presence of NO. *J. Geophys. Res.* **2002**, *107*, 4268.

(17) Chen, X.; Hulbert, D.; Shepson, P. B. Measurement of the Organic Nitrate Yield from OH Reaction with Isoprene. *J. Geophys. Res.* **1998**, *103*, 25563−25568.

(18) Paulot, F.; Crounse, J. D.; Kjaergaard, H. G.; Kroll, J. H.; Seinfeld, J. H.; Wennberg, P. O. Isoprene Photooxidation: New Insights into the Production of Acids and Organic Nitrates. *Atmos. Chem. Phys.* **2009**, *9*, 1479−1501.

(19) Horowitz, L. W.; Fiore, A. M.; Milly, G. P.; Cohen, R. C.; Perring, A.; Wooldridge, P. J.; Hess, P. G.; Emmons, L. K.; Lamarque, J.-F. Observational Constraints on the Chemistry of Isoprene Nitrates over the Eastern United States. *J. Geophys. Res.* **2007**, *112*, 1−13.

(20) Xie, Y.; Paulot, F.; Carter, W. P. L.; Nolte, C. G.; Luecken, D. J.; Hutzell, W. T.; Wennberg, P. O.; Cohen, R. C.; Pinder, R. W. Understanding the Impact of Recent Advances in Isoprene Photooxidation on Simulations of Regional Air Quality. *Atmos. Chem. Phys.* **2013**, *13*, 8439−8455.

(21) Rollins, A. W.; Browne, E. C.; Min, K. E.; Pusede, S. E.; Wooldridge, P. J.; Gentner, D. R.; Goldstein, a. H.; Liu, S.; Day, D. a.; Russell, L. M.; et al. Evidence for NO_x Control over Nighttime SOA Formation. *Science* **2012**, *337*, 1210−1212.

(22) Stone, D.; Whalley, L. K.; Heard, D. E. Tropospheric OH and HO_2 Radicals: Field Measurements and Model Comparisons. *Chem. Soc. Rev.* **2012**, *41*, 6348−6404.

(23) Mao, J.; Ren, X.; Zhang, L.; Van Duin, D. M.; Cohen, R. C.; Park, J.-H.; Goldstein, A. H.; Paulot, F.; Beaver, M. R.; Crounse, J. D.; et al. Insights into Hydroxyl Measurements and Atmospheric Oxidation in a California Forest. *Atmos. Chem. Phys.* **2012**, *12*, 8009−8020.

(24) Bouvier-Brown, N. C.; Goldstein, A. H.; Gilman, J. B.; Kuster, W. C.; de Gouw, J. A. In-situ Ambient Quantification of Monoterpenes, Sesquiterpenes, and Related Oxygenated Compounds during BEARPEX 2007: Implications for Gas- and Particle-Phase Chemistry. *Atmos. Chem. Phys.* **2009**, *9*, 5505−5518.

(25) Nguyen, T. B.; Crounse, J. D.; Schwantes, R. H.; Teng, A. P.; Bates, K. H.; Zhang, X.; St. Clair, J. M.; Brune, W. H.; Tyndall, G. S.; Keutsch, F. N.; et al. Overview of the Focused Isoprene eXperiment at the California Institute of Technology (FIXCIT): Mechanistic Chamber Studies on the Oxidation of Biogenic Compounds. *Atmos. Chem. Phys.* **2014**, *14*, 13531−13549.

(26) Liu, Y. J.; Herdlinger-Blatt, I.; McKinney, K. A.; Martin, S. T. Production of Methyl Vinyl Ketone and Methacrolein via the Hydroperoxyl Pathway of Isoprene Oxidation. *Atmos. Chem. Phys.* **2013**, *13*, 5715−5730.

(27) Rivera-Rios, J. C.; Nguyen, T. B.; Crounse, J. D.; Jud, W.; St. Clair, J. M.; Mikoviny, T.; Gilman, J. B.; Lerner, B. M.; Kaiser, J. B.; Gouw, J. d.; et al. Conversion of Hydroperoxides to Carbonyls in Field and Laboratory Instrumentation: Observational Bias in Diagnosing Pristine versus Anthropogenically Controlled Atmospheric Chemistry. *Geophys. Res. Lett.* **2014**, *41*, 8645−8651.

(28) Drewnick, F.; Hings, S. S.; DeCarlo, P. F.; Jayne, J. T.; Gonin, M.; Fuhrer, K.; Weimer, S.; Jimenez, J. L.; Demerjian, K. L.; Borrmann, S.; et al. A New Time-of-Flight Aerosol Mass Spectrometer (TOF-AMS)—Instrument Description and First Field Deployment. *Aerosol Sci. Technol.* **2005**, *39*, 637−658.

(29) DeCarlo, P. F.; Kimmel, J. R.; Trimborn, A.; Northway, M. J.; Jayne, J. T.; Aiken, A. C.; Gonin, M.; Fuhrer, K.; Horvath, T.; Docherty, K. S.; et al. Field-Deployable, High-Resolution, Time-of-Flight Aerosol Mass Spectrometer. *Anal. Chem.* **2006**, *78*, 8281−8289.

(30) Canagaratna, M. R.; Jimenez, J. L.; Kroll, J. H.; Chen, Q.; Kessler, S. H.; Massoli, P.; Hildebrandt Ruiz, L.; Fortner, E.; Williams, L. R.; Wilson, K. R.; et al. Elemental Ratio Measurements of Organic Compounds Using Aerosol Mass Spectrometry: Characterization, Improved Calibration, and Implications. *Atmos. Chem. Phys.* **2015**, *15*, 253−272.

(31) Nguyen, T. B.; Coggon, M. M.; Bates, K. H.; Zhang, X.; Schwantes, R. H.; Schilling, K. A.; Loza, C. L.; Flagan, R. C.;

DOI: 10.1021/acs.jpca.5b06355
J. Phys. Chem. A 2015, 119, 10158−10171

Wennberg, P. O.; Seinfeld, J. H. Organic Aerosol Formation from the Reactive Uptake of Isoprene Epoxydiols (IEPOX) onto Non-Acidified Inorganic Seeds. *Atmos. Chem. Phys.* **2014**, *14*, 3497−3510.
(32) St. Clair, J. M.; McCabe, D. C.; Crounse, J. D.; Steiner, U.; Wennberg, P. O. Chemical Ionization Tandem Mass Spectrometer for the in Situ Measurement of Methyl Hydrogen Peroxide. *Rev. Sci. Instrum.* **2010**, *81*, 094102−094102.
(33) Paulot, F.; Crounse, J. D.; Kjaergaard, H. G.; Kürten, A.; St. Clair, J. M.; Seinfeld, J. H.; Wennberg, P. O. Unexpected Epoxide Formation in the Gas-Phase Photooxidation of Isoprene. *Science* **2009**, *325*, 730−733.
(34) Crounse, J. D.; McKinney, K. A.; Kwan, A. J.; Wennberg, P. O. Measurement of Gas-Phase Hydroperoxides by Chemical Ionization Mass Spectrometry. *Anal. Chem.* **2006**, *78*, 6726−6732.
(35) Bates, K. H.; Crounse, J. D.; St. Clair, J. M.; Bennett, N. B.; Nguyen, T. B.; Seinfeld, J. H.; Stoltz, B. M.; Wennberg, P. O. Gas Phase Production and Loss of Isoprene Epoxydiols. *J. Phys. Chem. A* **2014**, *118*, 1237−1246.
(36) Teng, A. P.; Crounse, J. D.; Lee, L.; St. Clair, J. M.; Cohen, R. C.; Wennberg, P. O. Hydroxy Nitrate Production in the OH-Initiated Oxidation of Alkenes. *Atmos. Chem. Phys.* **2015**, *15*, 4297−4316.
(37) Praske, E.; Crounse, J. D.; Bates, K. H.; Kurten, T.; Kjaergaard, H. G.; Wennberg, P. O. Atmospheric Fate of Methyl Vinyl Ketone: Peroxy Radical Reactions with NO and HO_2. *J. Phys. Chem. A* **2015**, *119*, 4562−4572.
(38) Lee, L.; Teng, A. P.; Wennberg, P. O.; Crounse, J. D.; Cohen, R. C. On Rates and Mechanisms of OH and O_3 Reactions with Isoprene-Derived Hydroxy Nitrates. *J. Phys. Chem. A* **2014**, *118*, 1622−1637.
(39) Ng, N. L.; Kwan, A. J.; Surratt, J. D.; Chan, A. W. H.; Chhabra, P. S.; Sorooshian, A.; Pye, H. O. T.; Crounse, J. D.; Wennberg, P. O.; Flagan, R. C.; et al. Secondary Organic Aerosol (SOA) Formation from Reaction of Isoprene with Nitrate Radicals (NO_3). *Atmos. Chem. Phys.* **2008**, *8*, 4117−4140.
(40) Compernolle, S.; Ceulemans, K.; Muller, J. F. EVAPORATION: A New Vapour Pressure Estimation Method for Organic Molecules Including Non-Additivity and Intramolecular Interactions. *Atmos. Chem. Phys.* **2011**, *11*, 9431−9450.
(41) Skov, H.; Hjorth, J.; Lohse, C.; Jensen, N. R.; Restelli, G. Products and Mechanisms of the Reactions of the Nitrate Radical (NO_3) with Isoprene, 1,3-Butadiene and 2,3-Dimethyl-1,3-Butadiene in Air. *Atmos. Environ., Part A* **1992**, *26A*, 2771−2783.
(42) Berndt, T.; Boge, O. Gas-Phase Reaction of NO_3 Radicals with Isoprene: A Kinetic and Mechanistic Study. *Int. J. Chem. Kinet.* **1997**, *29*, 755−765.
(43) Suh, I.; Lei, W.; Zhang, R. Experimental and Theoretical Studies of Isoprene Reaction with NO_3. *J. Phys. Chem. A* **2001**, *105*, 6471−6478.
(44) Jenkin, M. E.; Hayman, G. D. Kinetics of Reactions of Primary, Secondary and Tertiary B-Hydroxy Peroxyl Radicals: Application to Isoprene Degradation. *J. Chem. Soc., Faraday Trans.* **1995**, *91*, 1911−1922.
(45) Zhao, J.; Zhang, R. A Theoretical Investigation of Nitrooxyalkyl Peroxy Radicals from NO_3-Initiated Oxidation of Isoprene. *Atmos. Environ.* **2008**, *42*, 5849−5858.
(46) Peeters, J.; Nguyen, T. L.; Vereecken, L. HO_x Radical Regeneration in the Oxidation of Isoprene. *Phys. Chem. Chem. Phys.* **2009**, *11*, 5935−5939.
(47) Peeters, J.; Müller, J.-F.; Stavrakou, T.; Nguyen, V. S. Hydroxyl Radical Recycling in Isoprene Oxidation Driven by Hydrogen Bonding and Hydrogen Tunneling: The Upgraded LIM1Mechanism. *J. Phys. Chem. A* **2014**, *118*, 8625−8643.
(48) Brown, S. S.; Stutz, J. Nighttime Radical Observations and Chemistry. *Chem. Soc. Rev.* **2012**, *41*, 6405−6447.
(49) Jenkin, M. E.; Boyd, A. A.; Lesclaux, R. Peroxy Radical Kinetics Resulting from the OH-Initiated Oxidation of 1, 3-Butadiene, 2, 3-Dimethyl-1, 3-Butadiene and Isoprene. *J. Atmos. Chem.* **1998**, *29*, 267−298.
(50) Saunders, S. M.; Jenkin, M. E.; Derwent, R. G.; Pilling, M. J. Protocol for the Development of the Master Chemical Mechanism, MCMv3 (Part A): Tropospheric Degradation of Non-Aromatic Volatile Organic Compounds. *Atmos. Chem. Phys.* **2003**, *3*, 161−180.
(51) Murrells, T. P.; Jenkin, M. E.; Shalliker, S. J.; Hayman, G. D. Laser Flash Photolysis Study of the UV Spectrum and Kinetics of Reactions of $HOCH_2CH_2O_2$ Radicals. *J. Chem. Soc., Faraday Trans.* **1991**, *87*, 2351−2360.
(52) Crowley, J. N.; Moortgat, G. K. 2-Bromoethylperoxy and 2-Bromo-1 -Methylpropylperoxy Radicals: Ultraviolet Absorption Spectra and Self-Reaction Rate Constants at 298 K. *J. Chem. Soc., Faraday Trans.* **1992**, *88*, 2437−2444.
(53) Mao, J.; Paulot, F.; Jacob, D. J.; Cohen, R. C.; Crounse, J. D.; Wennberg, P. O.; Keller, C. A.; Hudman, R. C.; Barkley, M. P.; Horowitz, L. W. Ozone and Organic Nitrates over the Eastern United States: Sensitivity to Isoprene Chemistry. *J. Geophys. Res.: Atmos.* **2013**, *118*, 11256−11258.
(54) Sulbaek Andersen, M. P.; Hurley, M. D.; Wallington, T. J.; Ball, J. C.; Martin, J. W.; Ellis, D. A.; Mabury, S. A. Atmospheric Chemistry of C_2F_5CHO: Mechanism of the $C_2F_5C(O)O_2$+HO_2 Reaction. *Chem. Phys. Lett.* **2003**, *381*, 14−21.
(55) Hasson, A. S.; Tyndall, G. S.; Orlando, J. J. A Product Yield Study of the Reaction of HO_2 Radicals with Ethyl Peroxy ($C_2H_5O_2$), Acetyl Peroxy ($CH_3C(O)O_2$), and Acetonyl Peroxy ($CH_3C(O)CH_2O_2$) Radicals. *J. Phys. Chem. A* **2004**, *108*, 5979−5989.
(56) Hurley, M. D.; Ball, J. C.; Wallington, T. J.; Sulbaek Andersen, M. P.; Nielsen, O. J.; Ellis, D. A.; Martin, J. W.; Mabury, S. A. Atmospheric Chemistry of n-C_xF_{2x+1} $CHO_{(x=1, 2, 3, 4)}$: Fate of n-$C_xF_{2x+1}C(O)$ Radicals. *J. Phys. Chem. A* **2006**, *110*, 12443−12447.
(57) Jenkin, M. E.; Hurley, M. D.; Wallington, T. J. Investigation of the Radical Product Channel of the CH_3COO_2 + HO_2 Reaction in the Gas Phase. *Phys. Chem. Chem. Phys.* **2007**, *9*, 3149−3162.
(58) Dillon, T. J.; Crowley, J. N. Direct Detection of OH Formation in the Reactions of HO_2 with $CH_3C(O)O_2$ and Other Substituted Peroxy Radicals. *Atmos. Chem. Phys.* **2008**, *8*, 4877−4889.
(59) Hasson, A. S.; Tyndall, G. S.; Orlando, J. J.; Singh, S.; Hernandez, S. Q.; Campbell, S.; Ibarra, Y. Branching Ratios for the Reaction of Selected Carbonyl-Containing Peroxy Radicals with Hydroperoxy Radicals. *J. Phys. Chem. A* **2012**, *116*, 6264−6281.
(60) Jenkin, M. E.; Hurley, M. D.; Wallington, T. J. Investigation of the Radical Product Channel of the $CH_3OCH_2O_2$ + HO_2 Reaction in the Gas Phase. *J. Phys. Chem. A* **2010**, *114*, 408−416.
(61) Hou, H.; Deng, L.; Li, J.; Wang, B. A Systematic Computational Study of the Reactions of HO_2 with RO_2: The HO_2 + CH_2ClO_2, $CHCl_2O_2$, and CCl_3O_2 Reactions. *J. Phys. Chem. A* **2005**, *109*, 9299−9309.
(62) Hou, H.; Wang, B. A Systematic Computational Study on the Reactions of HO_2 with RO_2: The HO_2 + CH_3O_2(CD_3O_2) and HO_2 + CH_2FO_2 Reactions. *J. Phys. Chem. A* **2005**, *109*, 451−460.
(63) St. Clair, J. M.; Rivera, J. C.; Crounse, J. D.; Knap, H. C.; Bates, K. H.; Teng, A. P.; Jorgensen, S.; Kjaergaard, H. G.; Keutsch, F. N.; Wennberg, P. O. Kinetics and Products of the Reaction of the First-Generation Isoprene Hydroxy Hydroperoxide (ISOPOOH) with OH. *J. Phys. Chem. A* **2015**.
(64) Crounse, J. D.; Knap, H. C.; Ørnsø, K. B.; Jørgensen, S.; Paulot, F.; Kjaergaard, H. G.; Wennberg, P. O. Atmospheric Fate of Methacrolein. 1. Peroxy Radical Isomerization Following Addition of OH and O_2. *J. Phys. Chem. A* **2012**, *116*, 5756−5762.
(65) Muller, J. F.; Peeters, J.; Stavrakou, T. Fast Photolysis of Carbonyl Nitrates from Isoprene. *Atmos. Chem. Phys.* **2014**, *14*, 2497−2508.
(66) Nguyen, T. B.; Crounse, J. D.; Teng, A. P.; St. Clair, J. M.; Paulot, F.; Wolfe, G. M.; Wennberg, P. O. Rapid Deposition of Oxidized Biogenic Compounds to a Temperate Forest. *Proc. Natl. Acad. Sci. U. S. A.* **2015**, *112*, E392−E401.
(67) Jacobs, M. I.; Burke, W. J.; Elrod, M. J. Kinetics of the Reactions of Isoprene-Derived Hydroxynitrates: Gas Phase Epoxide Formation and Solution Phase Hydrolysis. *Atmos. Chem. Phys.* **2014**, *14*, 8933−8946.
(68) Peeters, J.; Muller, J. F. HO_x Radical Regeneration in Isoprene Oxidation via Peroxy Radical Isomerizations. II: Experimental

DOI: 10.1021/acs.jpca.5b06355
J. Phys. Chem. A 2015, 119, 10158−10171

Evidence and Global Impact. *Phys. Chem. Chem. Phys.* **2010**, *12*, 14227−14235.
(69) Wolfe, G. M.; Crounse, J. D.; Parrish, J. D.; St. Clair, J. M.; Beaver, M. R.; Paulot, F.; Yoon, T. P.; Wennberg, P. O.; Keutsch, F. N. Photolysis, OH Reactivity and Ozone Reactivity of a Proxy for Isoprene-Derived Hydroperoxyenals (HPALDs). *Phys. Chem. Chem. Phys.* **2012**, *14*, 7276−7286.
(70) Surratt, J. D.; Chan, a. W. H.; Eddingsaas, N. C.; Chan, M. N.; Loza, C. L.; Kwan, a. J.; Hersey, S. P.; Flagan, R. C.; Wennberg, P. O.; Seinfeld, J. H. Reactive Intermediates Revealed in Secondary Organic Aerosol Formation from Isoprene. *Proc. Natl. Acad. Sci. U. S. A.* **2010**, *107*, 6640−6645.
(71) Lin, Y.-H.; Zhang, Z.; Docherty, K. S.; Zhang, H.; Budisulistiorini, S. H.; Rubitschun, C. L.; Shaw, S. L.; Knipping, E. M.; Edgerton, E. S.; Kleindienst, T. E.; et al. Isoprene Epoxydiols as Precursors to Secondary Organic Aerosol Formation: Acid-Catalyzed Reactive Uptake Studies with Authentic Compounds. *Environ. Sci. Technol.* **2012**, *46*, 250−258.

DOI: 10.1021/acs.jpca.5b06355
J. Phys. Chem. A 2015, 119, 10158−10171